ELSEVIER

# Electron density profile calculation technique for Autoscala ionogram analysis

Carlo Scotto

*Istituto Nazionale di Geofisica e Vulcanologia, Via di Vigna Murata 605, 00143 Rome, Italy*

## Abstract

An electron density profile model with free parameters is introduced. Initially the parameters are calculated on the basis of the ionospheric characteristics automatically obtained from the ionograms by Autoscala and considering the helio-geophysical conditions. The technique used to adjust the free parameters to the particular ionograms recorded is presented.
© 2009 COSPAR. Published by Elsevier Ltd. All rights reserved.

*Keywords:* Ionosphere; Ionogram; Electron density; Monitoring; Modelling

## 1. Introduction

The INGV (Istituto Nazionale di Geofisica e Vulcanologia) developed Autoscala, a computer program for the automatic scaling of the critical frequency $f_oF_2$ and $MUF(3000)F_2$ from ionograms (Scotto and Pezzopane, 2002; Pezzopane and Scotto, 2004, 2005, 2007). Autoscala was recently extended with the addition of a routine for the automatic scaling of the sporadic-$E$ layer (Scotto and Pezzopane, 2007) and a routine for the $F_1$ layer (Pezzopane and Scotto, 2008). Autoscala determines analytical functions for the $F_1$ and $F_2$ layers using an image recognition technique and can operate without polarization information. Autoscala was designed to be applied to the ionosonde AIS (Advanced Ionospheric Sounder), developed at the INGV. AIS is characterized by minimum transmitted power (less than 200 W) and consequently less weight, size, power consumption, and hardware complexity (Zuccheretti et al.; 2003; Bianchi et al., 2003).

The AIS–ING software required expansion to include a routine for the real time computation of the electron density profile, which is essential for ionospheric monitoring and space weather applications.

The two computer programs widely used at present are POLAN (Titheridge, 1985) and NhPC, the latter included in the Digisonde Data processing system ARTIST (Huang and Reinisch, 1996). These programs were developed more than 20 years ago and apply polynomial inversion techniques on the ionogram trace.

The POLAN program uses polynomial real-height sections of any required degree, fitting any number of data points with a weighted least-squares solution. It provides a procedure with adjustable resolution and it is able to mix physically desirable conditions with observed data.

The NhPC program expresses the $N(h)$ profile of each ionospheric layer with shifted Chebyshev polynomials. These polynomials are used with a logarithmic argument containing the plasma starting frequency and the critical frequency of each layer. The problem arising from the possible missing $h'(f)$ data points at the beginning of a trace is addressed by analytical expansion in the true height (profile) domain rather than by direct extrapolation of the $h'(f)$ trace. The validity of the Digisonde NhPC profiles was verified by comparison with incoherent scatter radar profiles (Huang and Reinisch, 1996).

Recently an iterative ray-tracing approach was also introduced in order to update the parameters of a three-dimensional electron density model that takes into account the horizontal gradients and general tilts. This approach is

*E-mail address:* scotto@ingv.it

implemented in a program named NeXtYZ, pronounced "next wise" (Zabotin et al., 2006).

This paper describes a technique for automatically estimating the electron density profile, adjusting the parameters of a model according to the recorded ionogram. Polan and NhPC start with a scaled (manual or auto) ionogram trace, $h'(f)$, and derive a plasma frequency profile from the first frequency up to $f_oF_2$. The revised Autoscala presented here derives a number of characteristics from the ionogram, not the whole trace, and then determines from a range of possible solutions the profile that best matches the scaled characteristics. The starting point for the model used in this work is the existing electron concentration models that use ionospheric parameters scaled from ionograms to generate a profile by means of mathematical expressions.

The model has a structure designed to limit time calculation. It uses the Reinisch and Huang (2000) formulation for the bottom-side $F_2$ profile and the $F_1$ layer, this results in a similarity with the International Reference Ionosphere (Bilitza and Reinisch, 2008).

## 2. An electron density profile model with free parameters

Fig. 1 shows a sketch of the electron density profile model, used in this work. It can be divided into the following two regions:

1) the bottom-side $F_2$ profile, through the $F_1$ layer to the top of the $E$ valley (from A to C, in Fig. 1);
2) the $E$ valley and the $E$ bottom-side (from C to F, in Fig. 1).

### 2.1. The bottom-side $F_2$ profile and the $F_1$ layer

This part of the profile is built on the basis of the formulation for the presentation of the $F_1$ layer in the IRI electron density profile from Reinisch and Huang (2000).

In their work this region is modelled defining the position of the anchor point A (see Fig. 1) with electron density $N_mF_2'$ and height $h_mF_2'$. The profile is completely defined introducing three shape parameters $B_0'$, $B_1'$, $D_1'$ and using the maximum electron density of the $F_1$ layer, $N_mF_1'$.

### 2.2. The E region modelling: the E valley and the E bottom-side

The $E$ region is modelled by defining the position of the following four anchor points (see Fig. 1):

a) the top valley point (point C), having electron density $N_mE'$ and height $h_mE' + \delta h_vE'$;
b) the valley point (point D), having electron density $N_mE' - \delta N_vE'$ and height $h_mE' + \delta h_vE'$;
c) the point (point E), having electron density $N_mE'$ and height $h_mE'$;
d) the zero point (point F), having electron density set to zero and height $h_mE'$-$y_mE'$.

The point C is joined to the point D by a parabola. This parabola is calculated by requiring a vertical slope at D, and continuity at points D and C. The point D is joined to the point E by a cubic. This cubic is calculated by requiring continuity and vertical slopes at the points D and E. The bottom-side of the E region (from the point E to the point F) is modelled by a parabolic layer.

### 2.3. The free parameters in the electron density profile model

Using the models for the $F_2 - F_1$ layers and the model for $E$ region described above, it is possible to build up an electron density profile model with 12 free parameters (6 related to the $E$ region and 6 to $F_2 - F_1$ layers). These parameters in the previous paragraphs were denoted with the apexes and are summarized below:

1) $N_mF_2'$ maximum electron density of $F_2$ layer;
2) $h_mF_2'$ height of the maximum electron density of $F_2$ layer;



A-C Reinisch and Huang (2000) formulation for intermediate, $F_1$ and $F_2$ regions
C-D polynomial of degree 2
D-E polynomial of degree 3
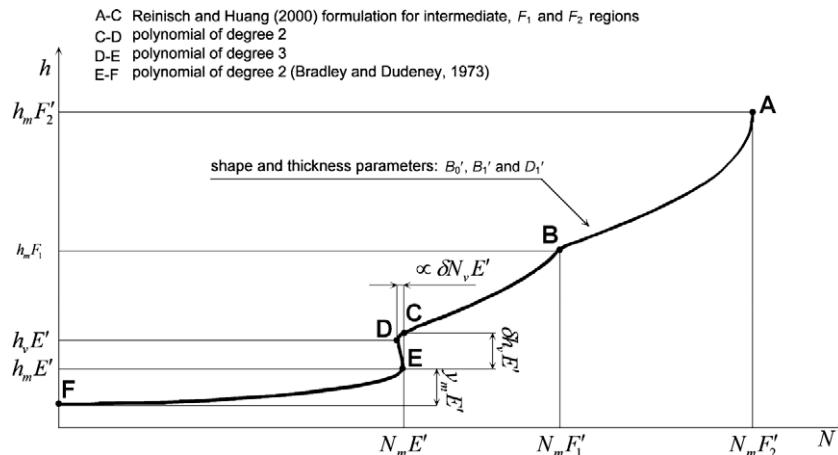E-F polynomial of degree 2 (Bradley and Dudeney, 1973)

Fig. 1. The electron density profile model used in this work. It can be divided into the following two regions: (1) the bottom-side $F_2$ profile, through the $F_1$ layer down to the top of the $E$ valley (from A to C); (2) the $E$ valley, and the $E$ bottom-side (from E to F).

3) $N_mF_1'$ maximum electron density of $F_1$ layer;
4) $B_0'$ thickness parameter;
5) $B_1'$ shape parameter;
6) $D_1'$ shape parameter;
7) $N_mE'$ maximum electron density of the $E$ layer;
8) $h_mE'$ height of the maximum electron density of $E$ layer;
9) $h_vE'$ height of the $E$ valley point;
10) $\delta h_vE'$ $E$ valley width;
11) $\delta N_vE'$ $E$ valley depth;
12) $y_mE'$ parabolic $E$ layer semi-thickness.

## 3. The algorithm for adjusting the model to the recorded ionogram

### 3.1. General features

Initially the data necessary for running the profile model are acquired. This is: the smoothed sunspot number $R_{12}$, the geomagnetic and geographic coordinates, the critical frequency of the $F_2$ region, the Maximum Usable Frequency for a distance of 3000 km, the information regarding the presence of an $F_1$ layer, and, as is the case, the critical frequency $f_oF_1$. The model described in the previous paragraph is able to describe a wide set of ionospheric profiles.

The basic idea of the procedure illustrated in this work consists of choosing the particular profile from this set that is able to give the best description of the ionosphere observed by the ionogram in question.

In Fig. 2 the flow chart of the algorithm is presented. The algorithm calculates the electron density profile from a model and from this profile computes a simulated ionogram. The parameters of the model $p_i$ are varied into appropriate ranges $\Delta p_i$ centred in the neighbourhood of some values $p_{i[\text{base}]}$ which are referred to as "base values" and which are modelled according to the input data. In this way a wide set of profiles is obtained and, from this, a corresponding set of simulated ionograms. Among these, the algorithm is able to select the ionogram that is most similar to the one recorded.

The range of variation of each parameter $p_i$ must be chosen also taking into account the calculation power available. In general, the greater the variation range of the parameter, the better the efficiency of the adjustment procedure, but the longer the required calculation time.

The most critical point in the algorithm is the comparison between the calculated ionogram and the real one. The choice of method applied strongly affects the performance and the required calculation time. In this work two different methods of comparison are used in two subsequent stages.

### 3.2. Calculation of the parameters for the approximate profile

The first step performed by the algorithm is the restriction of the set of profiles to those that are consistent with the parameters scaled by Autoscala and matching with the helio-geophysical conditions. The method used to estimate the base value of each parameter is shown below.

### 3.2.1. The maximum electron density of the $F_2$ layer $N_mF_{2[\text{base}]}$

This parameter is calculated from the autoscaled value of the critical frequency of the $F_2$ layer $f_oF_{2[\text{autoscaled}]}$, according to the relation

$$N_mF_{2[\text{base}]} = 1.24 \cdot 10^{10}(f_oF_{2[\text{autoscaled}]})^2, \tag{1}$$

where $f_oF_{2[\text{autoscaled}]}$ is expressed in MHz, while $N_mF_{2[\text{base}]}$ is expressed in m$^{-3}$.

### 3.2.2. The height of the maximum of the $F_2$ layer $h_mF_{2[\text{base}]}$

This parameter is calculated from the autoscaled value of the maximum usable frequency on a radio link of 3000 km, $MUF(3000)F_{2[\text{autoscaled}]}$, from $f_oF_{2[\text{autoscaled}]}$ and from the modelled value of the critical frequency of $E$ layer. The following relation is applied (Bradley and Dudeney, 1973):

$$h_mF_{2[\text{base}]} = \frac{1490}{M(3000)F_{2[\text{autoscaled}]} + \frac{0.18}{\frac{f_oF_{2[\text{autoscaled}]}}{f_oE_{[\text{modelled}]}} - 1.4}} - 176 \tag{2}$$

Where $M(3000)F_{2[\text{autoscaled}]} = MUF(3000)F_{2[\text{autoscaled}]}/f_oF_{2[\text{autoscaled}]}$, and $f_oE_{[\text{modelled}]}$, is a modelled value that will be defined in item 4).

### 3.2.3. The maximum electron density of the $F_1$ layer $N_mF_{1[\text{base}]}$

This parameter is calculated from the autoscaled value of the critical frequency of the $F_1$ layer $f_oF_{1[\text{autoscaled}]}$, according to the relation

$$N_mF_{1[\text{base}]} = 1.24 \cdot 10^{10} \cdot (f_oF_{1[\text{autoscaled}]})^2 \tag{3}$$

where $f_oF_{1[\text{autoscaled}]}$ is expressed in MHz, while $N_mF_{1[\text{base}]}$ is expressed in m$^{-3}$.

### 3.2.4. The shape parameter $B_{0[\text{base}]}$

The parameter $B_{0[\text{base}]}$ is calculated in two different ways, taking into account the information on the presence of the $F_1$ layer provided by Autoscala.

If Autoscala did not detect the presence of an $F_1$ cusp then we assume:

$$B_{0[\text{base}]} = h_mF_{2[\text{base}]} - h_{[\text{N}=\text{NmF2/e}]} \tag{4}$$

where

$$h_{[\text{N}=\text{NmF2/e}]} = h_mE_{[\text{base}]} + E_{\text{width}[\text{base}]} + \frac{(h_mF_{2[\text{base}]} - h_mE_{[\text{base}]} - E_{\text{width}[\text{base}]})}{N_mF_{2[\text{base}]} - N_mE_{[\text{base}]}} \cdot (N_mF_{2[\text{base}]}/\text{e} - N_mE_{[\text{base}]}) \tag{5}$$
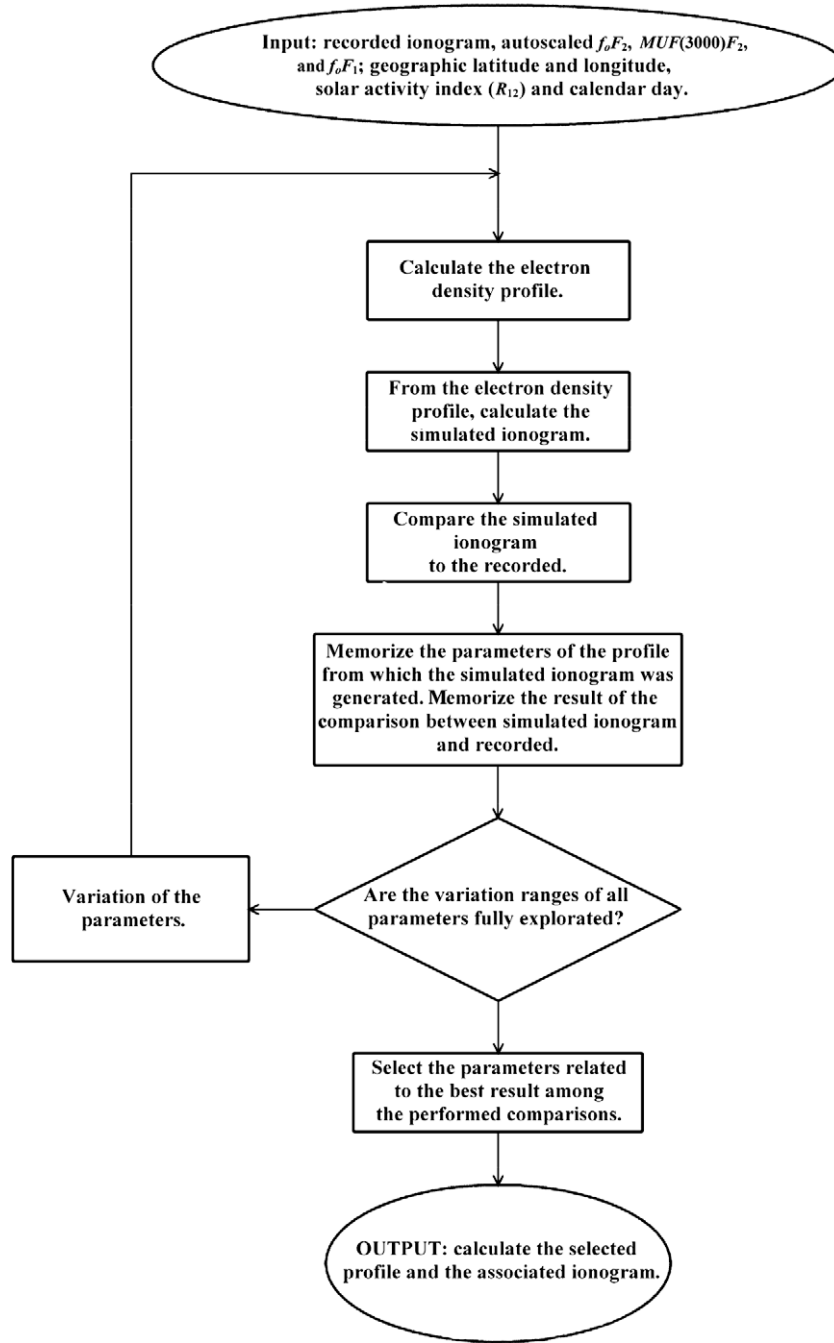
Fig. 2. The algorithm of the adjustment of the parameters of the electron density profile model to the recorded ionogram. The parameters $p_i$ of the model are varied into appropriate ranges $\Delta p_i$ centred in the neighbourhood of values $p_{i[base]}$. In this way a wide set of profiles is obtained and, from this, a corresponding set of simulated ionograms. Among these, the algorithm is able to select the ionogram that is most similar to the recorded one.

If Autoscala detected the presence of an $F_1$ cusp then we assume:

$$B_{0[base]} = \left(h_mF_{2[base]} - h_mF_{1[approx]}\right)\sqrt{\frac{N_mF_{2[base]}}{N_mF_{2[base]} - N_mF_{1[base]}}}$$

(6)

where

$$h_mF_{1[approx]} = (N_mF_{1[base]} - B)/A + 25\,\text{km},$$

(7)

With

$$A = \left(N_mF_{2[base]} - N_mE_{[base]}\right) / \left(h_mF_{2[base]} - h_mE_{[base]} - \delta h_vE_{[base]}\right)$$

and

$$B = N_mE_{[base]} - A \cdot h_mE_{[base]}.$$

### 3.2.5. The shape parameter $B_{1[base]}$

For the shape parameter $B_{1[base]}$ many numerical experiments were performed. They showed that it is sufficient to set $B_{1[base]} = 3$.

### 3.2.6. The Reinisch and Huang parameter $D_{1[\text{base}]}$

For the Reinisch and Huang (2000) shape parameter of $F_1$ region $D_{1[\text{base}]}$ it was set:

$$D_{1[\text{base}]} = 1.75 \quad \text{if Autoscala detected an } F_1 \text{ cusp} \tag{8}$$

$$D_{1[\text{base}]} = 0.35 \quad \text{if Autoscala did not detect an } F_1 \text{ cusp.} \tag{9}$$

The range of variation for these two parameters is rather critical. The present version of Autoscala is not able to separate the cases in which there is an inflection of the ionogram trace (L condition) from cases in which the $F_1$ region is completely absent. Consequently, the variation range of $D_1$ must be particularly large and was set $\Delta D_1 = 0.35$. In this way, if Autoscala did not detect an $F_1$ cusp, the allowed range of $D_1$ is from 0 to 0.70, including the cases in which the $F_1$ layer is completely absent together with the cases of L condition.

### 3.2.7. The maximum electron density of the E layer $N_mE_{[\text{base}]}$

The critical frequency of the E region $f_oE$ is modelled as a function of the solar zenith angle $\chi$, the smoothed sunspot number $R_{12}$, the geographic latitude $\lambda$, and the day number $D_y$:

$$f_0E_{\text{base}} = \begin{cases} 0.9 \cdot [(180 + 1.44 \cdot R_{12})\cos(\chi)]^{1/4} & \text{if } \chi < 80° \quad (10a) \\ a_{\text{trans}} + b_{\text{trans}} \cdot \chi & \text{if } 80° \le \chi < \chi_{\text{crit}} \quad (10b) \\ a_{\text{night}} + b_{\text{night}} \cdot \chi & \text{if } \chi \ge \chi_{\text{crit}} \quad (10c) \end{cases}$$

where $\chi_{\text{crit}}$ is $\chi$ associated with solar terminator at the altitude of the E layer, set to 110 km. The coefficients $a_{\text{trans}}$, $b_{\text{trans}}$, $a_{\text{night}}$ and $b_{\text{night}}$ are calculated through the following relations:

$$a_{\text{trans}} = [1.1459594 \cdot (180 + 1.44 \cdot R_{12})]/(180 + 1.44 \cdot R_{12})^{0.75}$$
$$+ 0.5815607 \cdot (180 + 1.44 \cdot R_{12})^{0.25}, \tag{11a}$$

$$b_{\text{trans}} = [-0.0143245 \cdot (180 + 1.44 \cdot R_{12})]/(180 + 1.44 \cdot R_{12})^{0.75} \tag{11b}$$

and

$$a_{\text{night}} = f_oE_{\text{crit}} - [(f_oE_{\text{crit}} - f_oE_{\text{midnight}})/(\chi_{\text{crit}} - \chi_{\text{midnight}})] \cdot \chi_{\text{crit}}, \tag{12a}$$

$$b_{\text{night}} = (f_oE_{\text{crit}} - foE_{\text{midnight}})/(\chi_{\text{crit}} - \chi_{\text{midnight}}) \tag{12b}$$

where

$$f_oE_{\text{crit}} = a_{\text{trans}} + b_{\text{trans}} \cdot \chi_{\text{crit}}, \tag{13a}$$

$$f_oE_{\text{midnight}} = [0.51 - 0.08 \sin(1.6 \cdot \lambda)] \cdot [1 + 0.06 \sin(D_y/58)]. \tag{13b}$$

The expression (10a) for $f_oE(\chi, R_{12})$ used for $\chi < 80°$ is due to Davies (1990), while the (13b) used to compute midnight value $f_oE_{\text{midnight}}$ is due to Titheridge (2000).

The variation of the modelled value of $f_oE$ dependence on $\chi$ is reported as an example in Fig. 3, for $\lambda = \pi/4$, $D_y = 100$ and $R_{12} = 100$.

### 3.2.8. The height of the maximum electron density of the E layer $h_mE_{[\text{base}]}$

The parameter $h_mE_{[\text{base}]}$ was fixed at 110 km under all conditions, as in the IRI model (Bilitza, 1998). The precision of this setting is sufficient in this context, although available data shows a dependence of this height on latitude, season, time and solar activity (Bilitza, 1998).
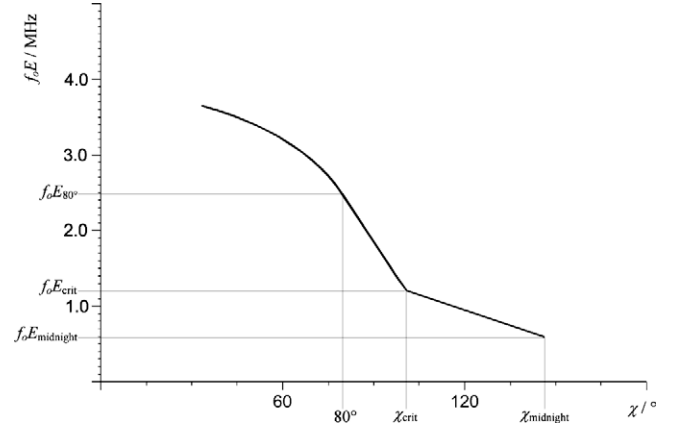


Fig. 3. The variation of the modelled value of $f_oE$ dependence on $\chi$ for $\lambda = \pi/4$, $D_y = 100$ and $R_{12} = 100$.

### 3.2.9. The height of the E valley $h_{E\text{valley}[\text{base}]}$

The height of the E valley, $h_{E\text{valley}[\text{base}]}$ is computed, as for $\delta h_vE_{[\text{base}]}$, by a model based on incoherent scatter radar measurements (Mahajan et al., 1997). According to this model $h_{E\text{valley}[\text{base}]}$ can be expressed as follows:

for $0° \le \chi \le 85°$, $h_{E\text{valley}} = 115.8 + 0.02 \cdot \chi$
$$+ 0.00078 \cdot \chi^2; \tag{14a}$$

for $85° \le \chi \le 180°$, $h_{E\text{valley}} = 130.73 - 0.069172 \cdot \theta$
$$+ 0.1429 \cdot 10^{-3} \cdot \theta^2, \tag{14b}$$

where $\theta = \chi$ before midnight and $\theta = 360 - \chi$ after midnight.

### 3.2.10. The width of E valley $\delta h_vE_{[\text{base}]}$

This parameter is calculated by a model based on incoherent scatter radar measurements (Mahajan et al., 1997). According to this model $\delta h_vE$ can be expressed as follows:

for $0° \le \chi \le 85°$, $\delta h_vE_{[\text{base}]} = 7.12 - 0.031 \cdot \chi$
$$+ 0.0023 \cdot \chi^2; \tag{15a}$$

for $85° \le \chi \le 180°$, $\delta h_vE_{[\text{base}]} = -329.4 + 6.04926 \cdot \theta +$
$$- 0.025269 \cdot \theta^2 + 0.00003005 \cdot \theta^3, \tag{15b}$$

where $\theta = \chi$ before midnight and $\theta = 360 - \chi$ after midnight.

### 3.2.11. The E valley depth $\delta N_vE'_{[\text{base}]}$

This parameter is also calculated by a model based on incoherent scatter radar measurements (Mahajan et al., 1997). According to this model the percentage depth can be calculated as follows:

for $0° \le \chi \le 85°$, $D_{\%E\text{valley}} = 0.96 - 0.00069 \cdot \chi$
$$+ 0.000034 \cdot \chi^2 - 0.0000006 \cdot \chi^3; \tag{16a}$$

for $85° \le \chi \le 180°$, $D_{\%E\text{valley}} = 8.9814 - 0.198225$
$$\cdot \theta + 0.001597 \cdot \theta^2 - 0.00000552 \cdot \theta^3 + 0.6953710^{-8} \cdot \theta^4, \tag{16b}$$

where $\theta = \chi$ before midnight and $\theta = 360 - \chi$ after midnight.

Therefore, for the $E$ valley depth, it follows that:

$$\delta N_v E'_{[\text{base}]} = D_{\%\text{Evalley}} \cdot N_m E_{[\text{base}]}.$$

### 3.2.12. The parabolic E layer semi-thickness $y_mE_{[\text{base}]}$

The $E$ layer semi-thickness was set $y_mE_{[\text{base}]} = 15$ km, as numerical experiments showed that this value worked slightly better than the original $y_mE_{[\text{base}]} = 20$ km (Bradley and Dudeney, 1973).

### 3.3. Calculation of the electron density profile

The electron density profile is calculated, using the model described in Section 2. This calculation is performed on the basis of the 12 parameters defined in Section 2.3. On the first loop the profile is the approximate one obtained setting each parameter to the base value, according to the formulas described in Section 3.2.

### 3.4. Calculation of the ionogram associated with the profile

For a horizontally stratified ionosphere, the virtual height $h'$ for a radio wave of frequency $f$ is given by:

$$h'(f) = \int_0^{h_R} n(f, f_p) \, dh, \tag{17}$$

$$h'(f) = \int_0^{h_R} n(f, f_p) \left( \frac{dh}{df_p} \right) df_p, \tag{18}$$

where $f_p$ is the plasma frequency at height $h$ in the ionosphere, and $f_r$ is the plasma frequency at the reflection height $h_R$. For the ordinary ray, $f_r$ is equal to the wave frequency $f$; for the extraordinary ray the reflection frequency is $f_r = (f(f - f_b))^{1/2}$ where $f_b$ is the electron gyrofrequency in the ionosphere. Here $n$ is the group refractive index, a complicated function of $f, f_p, f_b,$ and the magnetic dip angle.

### 3.5. Comparison of the calculated with the recorded ionogram: two methods of comparing a simulated ionograms with a real one

A possible solution to the problem of ionogram inversion can be based on a technique by which the root mean square error between the trace restored from a candidate profile and the recorded one is minimized. Such an approach is similar to the function approximations methods used in many branches of applied mathematics, and computer science in particular. In general, a function approximation problem is solved by selecting a function from among a well-defined class that closely matches ("approximates") a target function in a task-specific way. Therefore in the following this iterative minimization scheme will be referred as *target function method*.

Some iterative techniques had already been introduced to match the trace restored from a candidate profile with

the source ionogram. Wright et al. (1972) described a profile inversion procedure in which the optimum radio-frequency soundings intervals were specified from an approximate knowledge of the profile, estimating the expected virtual height $h'$ coordinate at this frequency $f$.

In NhPC (included in the ARTIST system) the extrapolation and interpolation through gaps due to missing $h(f)$ data is accomplished by computing the profile from the trace segments and from the computed profile back to the completed traces (Reinisch and Huang, 1983; Huang and Reinisch, 1996; Reinisch et al., 2005).

In developing the algorithm, two different methods of comparing a simulated ionogram with a real one were considered:

a) the target function method based on the root mean square error;
b) a method based on correlation, very similar to the method used in Autoscala (Scotto and Pezzopane, 2002; Pezzopane and Scotto, 2007). In principle, both methods permit the identification of the simulated ionogram that best approximates the recorded one. In this work, the two methods are used in two subsequent stages: first $M = 10^3$ simulated ionograms are selected from the initial set using method (a), then from among these $M = 10^3$ ionograms the best one is selected according to method (b).

The method (a) is based on the knowledge of some specific points that are determined as belonging to the ionogram trace with sufficient reliability (anchor points). As we will discuss extensively in Section 3.5.1, the anchor points can be determined by the analytical functions representing the $F_1$ and $F_2$ traces produced by Autoscala. Based on these reference points the root mean square error $\Delta_{[\text{recorded/simulated}]}$ is computed between the recorded ionogram and the simulated trace. A good fit between the two traces is expressed in this case by a low value $\Delta_{[\text{recorded/simulated}]}$. The main problem with this method is that reliable reference points must be available.

The second method consists in calculating the correlation between the recorded ionograms and the simulated one, based on the information available over the complete frequency range covered by the ionogram. The problem with this method is that it requires extended calculation time.

### 3.5.1. Comparison between simulated and real ionograms based on root mean square error

For each ionogram in which the recorded echo is sufficiently clear Autoscala is able to select an analytical function, $h_vF_2(f)$, which can be considered as representative of the $F_2$ trace. For daytime ionograms the automatic scaling of the $F_1$ trace is also attempted. Autoscala is able to recognise if the $F_1$ cusp is present and in this case fits a part of the trace with an analytical function, $h_vF_1(f)$. From $h_vF_2(f)$ and $h_vF_1(f)$ the critical frequencies of $F_2$ layer

$f_oF_{2[autoscaled]}$ and of $F_1$ layer $f_oF_{1[autoscaled]}$ are obtained respectively. In addition the following frequencies can be introduced:

1) $f_oF_{2[tra-beg]}$ (whether the $F_1$ layer is detected or not) defined as the frequency of the beginning of the range of extension of $h_v F_2(f)$;
2) $f_{[h'F2]}$ (if only the $F_1$ layer is detected) defined as the frequency at which $h'F_2$ is automatically scaled by Autoscala and it is obtained from the relative minimum of $h_v F_1(f)$.

Fig. 4 illustrates a typical ionogram showing the $F_2$ region only. For this kind of ionogram two anchor points are considered to compare the simulated ionogram to the recorded one:

(1) point $N_1$, at frequency $f_{[N1]} = (f_oF_{2[autoscaled]}$
$$+ f_oF_{2[tra-beg]})/2 \quad (19)$$
(2) point $N_2$, at frequency $f_{[N2]} = f_oF_{2[tra-beg]}$
$$+ 0.1\,\text{MHz} \quad (20)$$

Fig. 5 illustrates a typical ionogram showing both the $F_2$ and the $F_1$ regions. For this kind of ionogram three anchor points are considered to compare the simulated ionogram to the recorded one:

(1) point $Y_1$, at frequency $f_{[Y1]} = f_oF_{2[autoscaled]}$
$$- 0.5\,\text{MHz}; \quad (21)$$
(2) point $Y_2$, at frequency $f_{[Y2]} = f_{[h'F2]}$; $\quad (22)$
(3) point $Y_3$, at frequency $f_{[Y3]} = f_{[h'F2]} - 0.3\,\text{MHz}$. $\quad (23)$

Using the anchor points defined above (two points if there is no $F_1$ region, three points if there is an $F_1$ region), the root mean square error between the virtual heights of the simulated ionogram and the real one is calculated.

### 3.5.2. Comparison between simulated and real ionograms based on correlation

For each set of parameters $N_mF'_2$, $h_mF'_2$, $N_mF'_1$, $B'_0$, $B'_1$, $D'_1$, $N_mE'$, $h_mE'$, $h'_{vE}$, $\delta N'_{vE}$, $\delta h'_{vE}$, $y_mE'$ an electron density profile was derived and from this the corresponding simulated ionogram. For each simulated ionogram the correlation $C(N_mF'_2, h_mF'_2, N_mF'_1, B'_0, B'_1, D'_1, N_mE', h_mE', h'_{vE}, \delta N'_{vE}, \delta h'_{vE}, y'_{mE})$ with the recorded one is then calculated. Empirically, this method seems to be very effective, but, as said before, it requires extended calculation time. This is mainly due to the fact that it is necessary to calculate the complete ionogram trace.

### 3.6. Selection of the best profile

In order to reduce the calculation time, the selection of the best electron density profile is performed in two stages.

a) In the first stage the $10^3$ profiles that gave the best results in term of root mean square error are selected. As stated in Section 3.5.1, it is not necessary to calculate the complete ionogram trace which results in a drastic reduction in calculation time, consequently making it possible to consider a wide set of modelled profiles.
b) Among the $10^3$ ionograms mentioned above the one that gives the best result in terms of correlation is selected.

The complete procedure for the selection of the best profile is performed in 90 s on a PC equipped with a Pentium 4 CPU clocking at 3 GHz.

Examples are shown of the graphic outputs produced for typical mid-latitude ionograms with the $F_2$ region only (Fig. 6) and with both the $F_2$ and $F_1$ regions (Fig. 7). The ionogram reported in this figure also shows echoes from
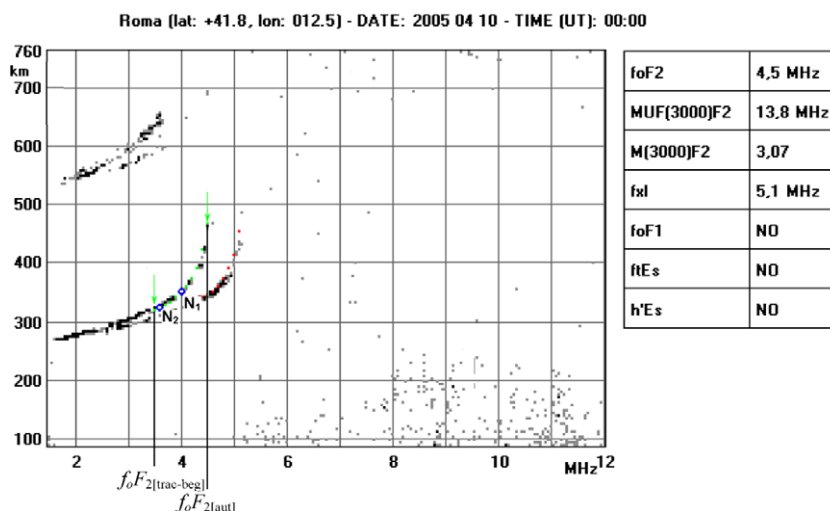


Fig. 4. A typical ionogram showing the $F_2$ region only. The points $N_1$ and $N_2$ used to compare the simulated ionogram to the recorded one are indicated. The green arrows indicate the beginning and the end of the $F_2$ ordinary trace detected by Autoscala.

Fig. 5. A typical ionogram showing both the $F_1$ and the $F_2$ regions. The points $Y_1$, $Y_2$, and $Y_3$ that are used to compare the simulated ionogram to the recorded one are indicated. The green arrows indicate the beginning 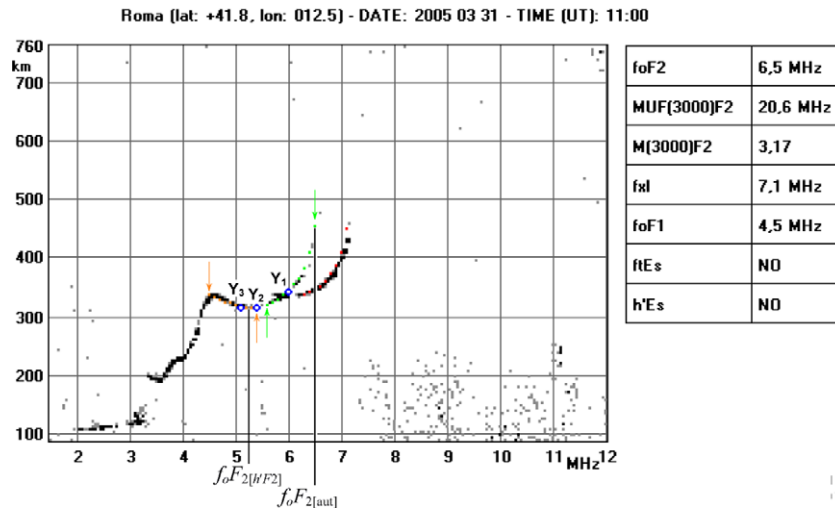and the end of the $F_2$ ordinary trace detected by Autoscala. The orange arrows indicate the beginning and the end of the $F_1$ ordinary trace detected by Autoscala.
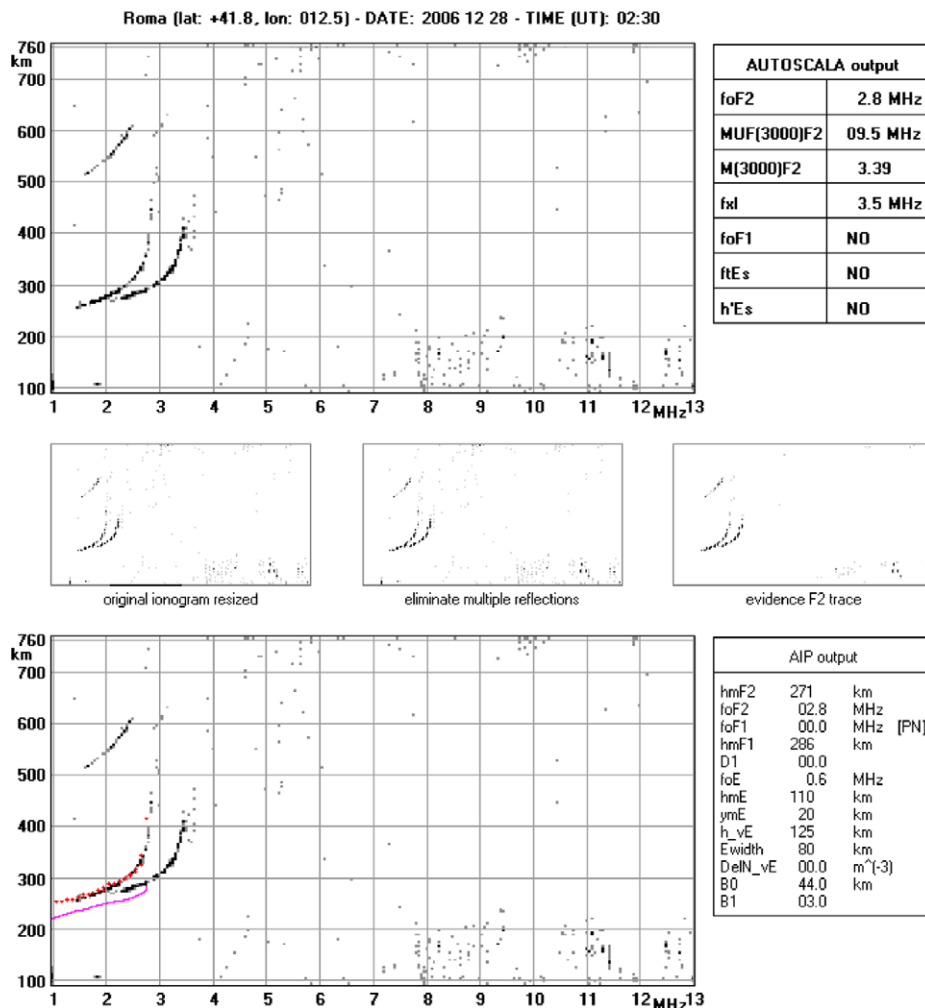


Fig. 6. An example of the graphic output produced applying the AIP for an ionogram in which only the $F_2$ region is observable.
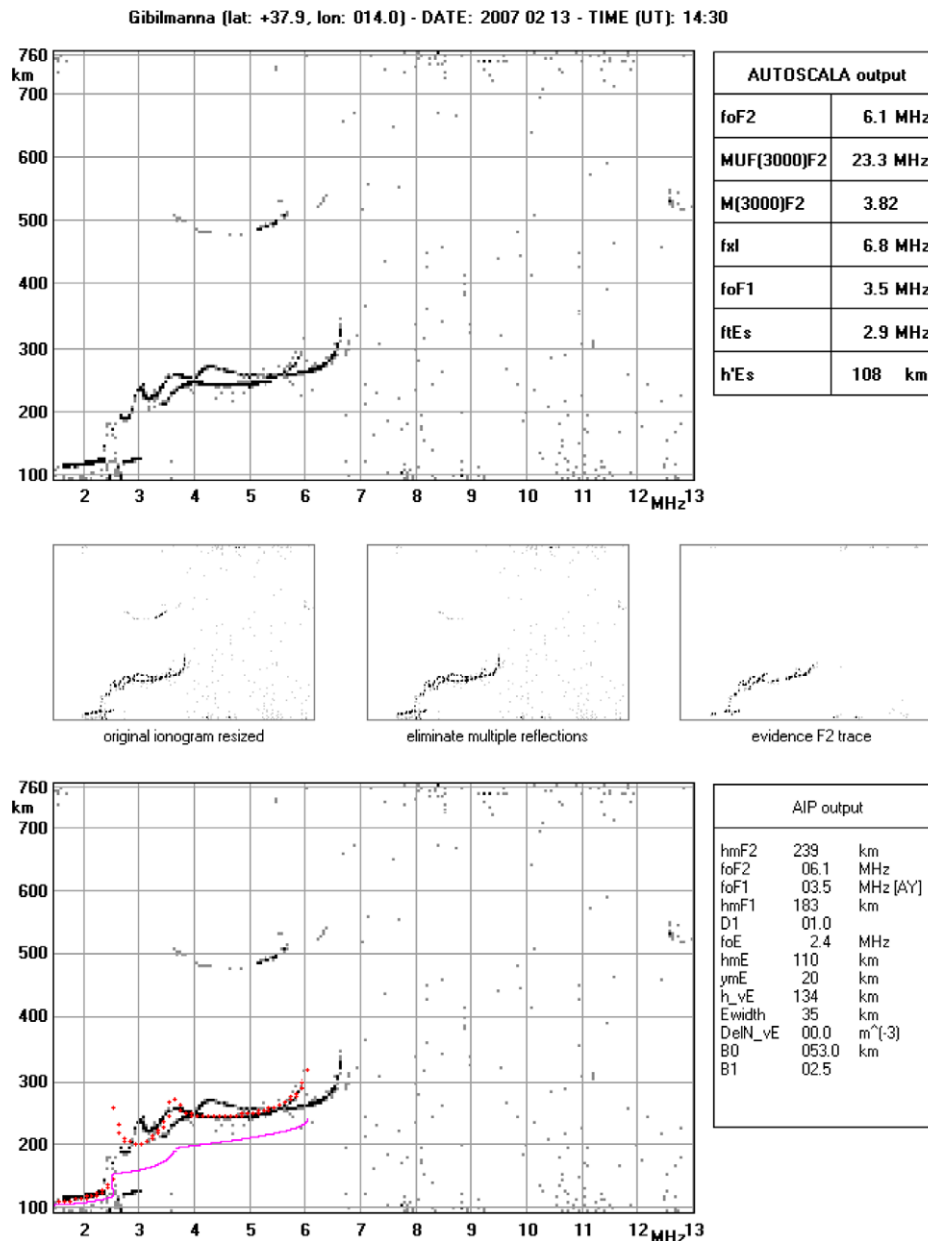
Gibilmanna (lat: +37.9, lon: 014.0) - DATE: 2007 02 13 - TIME (UT): 14:30



| AUTOSCALA output | |
|---|---|
| foF2 | 6.1 MHz |
| MUF(3000)F2 | 23.3 MHz |
| M(3000)F2 | 3.82 |
| fxI | 6.8 MHz |
| foF1 | 3.5 MHz |
| ftEs | 2.9 MHz |
| h'Es | 108 km |

original ionogram resized

eliminate multiple reflections

evidence F2 trace

| AIP output | | |
|---|---|---|
| hmF2 | 239 | km |
| foF2 | 06.1 | MHz |
| foF1 | 03.5 | MHz [AY'] |
| hmF1 | 183 | km |
| D1 | 01.0 | |
| foE | 2.4 | MHz |
| hmE | 110 | km |
| ymE | 20 | km |
| h_vE | 134 | km |
| Ewidth | 35 | km |
| DelN_vE | 00.0 | m^(-3) |
| B0 | 053.0 | km |
| B1 | 02.5 | |

Fig. 7. An example of the graphic output produced applying the AIP for an ionogram in which both the $F_2$ and $F_1$ regions are observable. This ionogram also shows echoes from multiple stratifications in the $E$-region. The model used in this work is not able to take into account these stratifications and so fit mismatches between the recorded and the restored trace are produced.

multiple stratifications in the $E$-region. The model used in this work is not able to take into account these stratifications. Therefore fit mismatches between the recorded and the restored trace are produced in the $E$ region.

Fig. 8 is an ionogram showing an $F_{1.5}$ layer, recorded by the AIS–INGV installed in the ionospheric station of Tucumán, Argentina, (26.9 S, 65.4 W), (Pezzopane et al., 2007). The system is not designed to identify this layer; the applied electron density profile model is too simple, consequently generating an unrealistic electron density profile. This stratification is seldom observed in the Mediterranean region but is very common at low latitude. Therefore the technique described in this work should be carefully

tested before considering application to ionosondes installed at equatorial regions.

## 4. Conclusions

The model developed in this work can be applied to ionograms for electron density profile calculation. It uses as input the main ionospheric parameters automatically scaled by Autoscala. The application of the electron density profile calculation technique illustrated in this work to the real time ionograms recorded and autoscaled by the AIS–INGV/Autoscala system installed at the stations of Gibilmanna (http://ionos.ingv.it/Gibilmanna/latest.
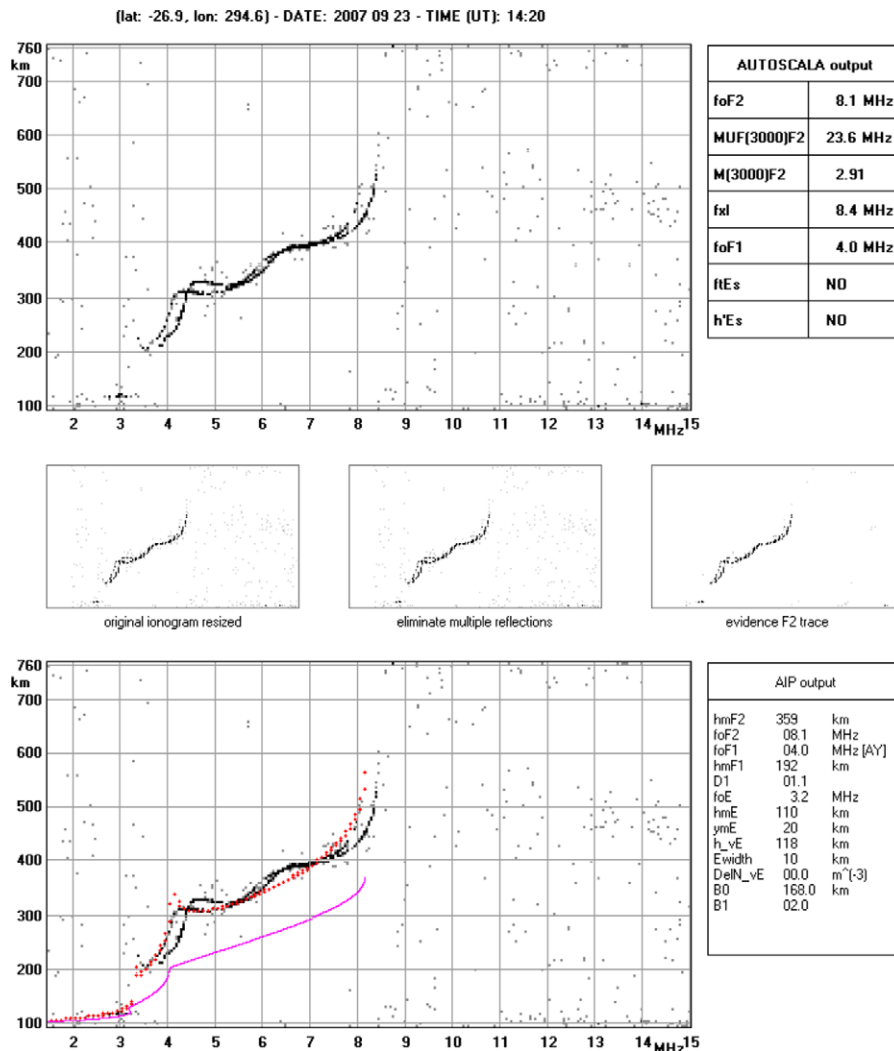
Fig. 8. An ionogram showing an $F_{1.5}$ layer recorded by the AIS–INGV installed in the ionospheric station of Tucumán, Argentina (26.9 S, 65.4 W). The system is not designed to identify this layer, the applied electron density profile model is too simple and an unrealistic electron density profile was consequently generated.

html) and Rome (http://ionos.ingv.it/Roma/latest.html) can be seen on the Internet.

A quantitative test of the performance of the system should be carried out for application to real time ionospheric monitoring, with special attention to equatorial latitudes. Nevertheless, the reasonably good match obtained in many cases between the recalculated traces and the measured ones inspires confidence in the method developed.

### References

Bianchi, C., Sciacca, U., Zirizzotti, A., Zuccheretti, E., Arokiasamy, B.J. Signal processing techniques for phase-coded HF-VHF radars. Ann. Geophys. 46, 697–705, 2003.

Bilitza, D. The E and D region in IRI. Adv. Space Res. 21, 871–878, 1998.

Bradley, P.A., Dudeney, J.R. Simple model of the vertical distribution of electron concentration in the ionosphere. J. Atmos. Terr. Phys. 35, 2131–2146, 1973.

Bilitza, D., Reinisch, B.W. International Reference Ionosphere 2007: improvements and new parameters. Adv. Space Res. 42, 599–609, 2008.

Davies, K. Ionospheric Radio. Peter Peregrinus Ltd., London, United Kingdom, 1990.

Huang, X., Reinisch, B.W. Vertical electron density profiles from the digisonde network. Adv. Space Res. 18 (6), 121–129, 1996.

Mahajan, K.K., Sethi, N.K., Pandey, V.K. The diurnal variation of E–F valley parameters from incoherent scatter measurement at Arecibo. Adv. Space Res. 20, 1781–1784, 1997.

Pezzopane, M., Scotto, C. Software for the automatic scaling of critical frequency foF2 and MUF(3000)F2 from ionograms applied at the Ionospheric Observatory of Gibilmanna. Ann. Geophys. 47, 1783–1790, 2004.

Pezzopane, M., Scotto, C. The INGV software for the automatic scaling of foF2 and MUF(3000)F2 from ionograms: a performance comparison with ARTIST 4.01 from Rome data. J. Atmos. Solar-Terr. Phys. 67, 1063–1073, 2005.

Pezzopane, M., Scotto, C. The automatic scaling of critical frequency foF2 and MUF(3000)F2: a comparison between Autoscala and ARTIST 4.5 on Rome data. Radio Sci. 42, RS4003, doi:10.1029/2006RS003581, 2007.

Pezzopane, M., Scotto, C. A method for automatic scaling of F1 critical frequency from ionograms. Radio Sci. 43, RS2S91, doi:10.1029/2007RS003723, 2008.

Pezzopane, M., Zuccheretti, E., Bianchi, C., Scotto, C., Zolesi, B., Cabrera, M.A., Ezquer, R.G. The new ionospheric station of Tucumán: first results. Ann. Geophys. 40, 49–483, 2007.

Reinisch, B.W., Huang, X. Automatic calculation of electron density profiles from digital ionograms 3. Processing of bottomside ionograms. Radio Sci. 18, 477–492, 1983.

Reinisch, B.W., Huang, X. Redefining the IRI F1 layer profile. Adv. Space Res. 25, 81–88, 2000.

Reinisch, B.W., Huang, X., Galkin, I.A., Paznukhov, V., Kozlov, A. Recent advances in real-time analysis of ionograms and ionospheric drift measurements with digisondes. J. Atmos. Solar-Terr. Phys. 67, 1054–1062, 2005.

Scotto, C., Pezzopane, M. A software for automatic scaling of foF2 and MUF(3000)F2 from ionograms. Proceedings of URSI 2002, Maastricht, 17–24 August, 2002 (on CD).

Scotto, C., Pezzopane, M. A method for automatic scaling of sporadic *E* layers from ionograms. Radio Sci. 42, RS2012, doi:10.1029/2006RS003461, 2007.

Titheridge, J.E., Ionogram analysis with the generalised program Polan, Report UAG-93. World Data Center A for Solar-Terrestrial Physics, NOAA, E/GC2, Boulder, CO 80303, 1985.

Titheridge, J.E. Modelling the peak of the ionospheric *E*-layer. J. Atmos. Solar-Terr. Phys. 62, 93–114, 2000.

Wright, J.M., Laird, A.R., Obitts, D., Violette, E.J., McKinnis, D. Automatic $N(h, t)$ profiles of the ionosphere with a digital ionosonde. Radio Sci. 7, 1033–1042, 1972.

Zabotin, N.A., Wright, J.W., Zhbankov, G.A. NeXtYz: three-dimensional electron density inversion for dynasonde ionograms. Radio Sci. 41, RS6S32, doi:10.1029/2005RS003352, 2006.

Zuccheretti, E., Tutone, G., Sciacca, U., Bianchi, C., Arokiasamy, B.J. The new AIS–INGV digital ionosonde. Ann. Geophys. 46, 647–659, 2003.